Bioinformatics, 38(2), 2022, 503–512
doi: 10.1093/bioinformatics/btab638
Advance Access Publication Date: 13 September 2021
Original Paper

OXFORD

Bioimage informatics

Image enhancement to leverage the 3D morphological reconstruction of single-cell neurons

Shuxia Guo , Xuan Zhao, Shengdian Jiang , Liya Ding* and Hanchuan Peng*

Institute for Brain and Intelligence, Southeast University, 210096 Nanjing, Jiangsu Province, China

*To whom correspondence should be addressed.

Associate Editor: Olga Vitek

Received on April 6, 2021; revised on August 5, 2021; editorial decision on August 7, 2021; accepted on September 9, 2021

Abstract

Motivation: To digitally reconstruct the 3D neuron morphologies has long been a major bottleneck in neuroscience. One of the obstacles to automate the procedure is the low signal-background contrast (SBC) and the large dynamic range of signal and background both within and across images.

Results: We developed a pipeline to enhance the neurite signal and to suppress the background, with the goal of high SBC and better within- and between-image homogeneity. The performance of the image enhancement was quantitatively verified according to the different figures of merit benchmarking the image quality. In addition, the method could improve the neuron reconstruction in approximately 1/3 of the cases, with very few cases of degrading the reconstruction. This significantly outperformed three other approaches of image enhancement. Moreover, the compression rate was increased five times by average comparing the enhanced to the raw image. All results demonstrated the potential of the proposed method in leveraging the neuroscience by providing better 3D morphological reconstruction and lower cost of data storage and transfer.

Availability and implementation: The study is conducted based on the Vaa3D platform and python 3.7.9. The Vaa3D platform is available on the GitHub (https://github.com/Vaa3D). The source code of the proposed image enhancement as a Vaa3D plugin, the source code to benchmark the image quality and the example image blocks are available under the repository of vaa3d_tools/hackathon/SGuo/imPreProcess. The original fMost images of mouse brains can be found at the BICCN's Brain Image Library (BIL) (https://www.brainimagelibrary.org).

Contact: h@braintell.org or dinglyosu@seu.edu.cn

Supplementary information: Supplementary data are available at *Bioinformatics* online.

1 Introduction

Digital neuron reconstruction has long been a major challenge and bottleneck in brain and neuroscience (Meijering, 2010; Svoboda, 2011). The current procedure of neuron reconstruction, despite supported by computer algorithms, mostly requires manual verification and correction, making it infamously time consuming and labor intensive. This adds a lot burden on the capacity of massive data management, which is necessary considering the fast growing data amount under the development of imaging techniques. It is hence an urgent need to automate the neuron reconstruction.

One major issue hampering the full automation of neuron reconstruction is that the image quality varies largely in terms of the signal-background contrast (SBC), the uniformity of the background and the density of labeled neuron cells, which are all important factors to neuron reconstruction algorithms (Zhou *et al.*, 2015). Such variations can be seen across different images and even among different regions of a single image. To give a general view of the situation, we collected in Figure 1 example 3D dendritic images of 'good', 'median' and 'poor' quality, where the 3D images were represented as the maximum intensity projection (MIP) along *z*-axis. The quality was graded via visual inspection. Images with denser neuron cells (i.e. neurite arbors), lower contrast and higher noise level were considered of poorer quality. Such large diversity of image quality puts extreme challenges in automatic neuron reconstruction as it is almost impossible to find an optimal parameter setting that fits all images. A dynamic procedure for parameter selection is always possible but can give vital errors especially for images of poor quality. As a consequence, the neuron reconstruction is prone to mistakes on images of poor quality or regions with obvious noise. To improve the image quality via techniques of image enhancement is thus considered as an effective way to push forward the automatic neuron reconstruction.

There exist a large number of techniques for image enhancement. With these procedures, it is expected to eliminate or reduce the influence from uneven background, low foreground–background contrast, low signal-to-noise ratio, etc. The denoising approaches range from simple filtering to more advanced methods like sparse coding

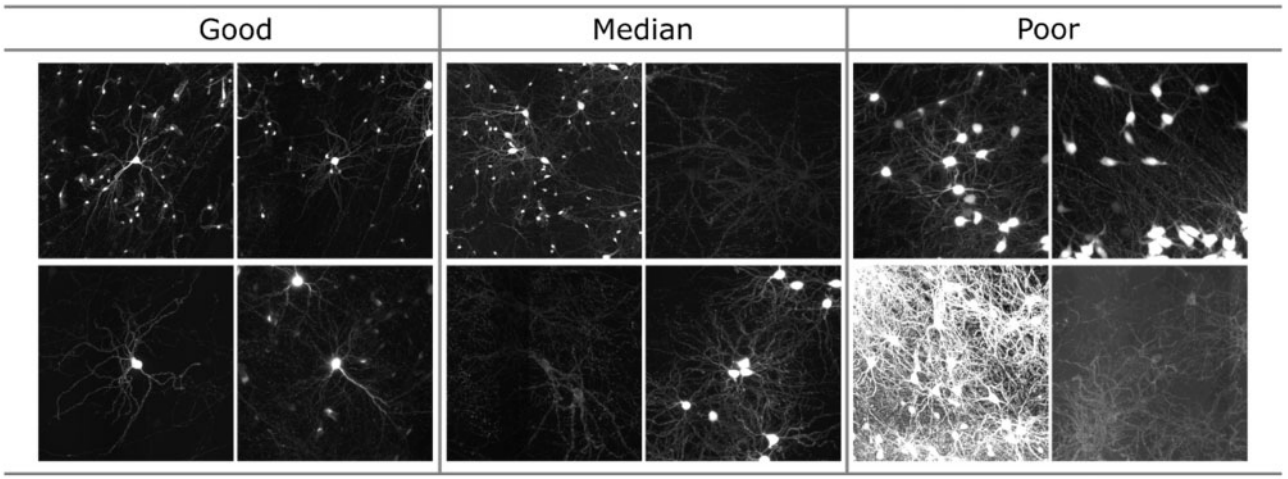

Fig. 1. Example dendritic images (in MIP) of different image quality. Images with denser neuron cells (i.e. neurite arbors), lower contrast and higher noise level were considered of poorer quality

technology, image self-similarity and low-rank decomposition (Dabov *et al.*, 2006; Xu *et al.*, 2018). Moreover, approaches are developed to handle the issue of uneven illumination in microscopic imaging, such as BaSiC, CIDRE and BAM (Chernavskaia *et al.*, 2017; Peng *et al.*, 2017; Smith *et al.*, 2015). Deep neural networks are being applied in image enhancement as well, such as the Content Sensing Image Restoration (CARE), N2V, PN2V, Noise2noise and Noise2Self, to name a few (Batson and Royer, 2019; Buchholz *et al.*, 2019; Krull *et al.*, 2020; Laine *et al.*, 2019; Lehtinen *et al.*, 2018; Zhu *et al.*, 2017). Methods are also reported specifically for the enhancement of neurite or fiber structures. For instance, a content aware neuron image enhancement (CaNE) method was proposed by formulating the task of image enhancement as an optimization problem with the restriction of the gradient sparsity and tubular structure of neuron images (Liang *et al.*, 2017). In other algorithms, the tubular structure of neurons is enhanced based on Hessian matrix, gray-scale image distance transform, Meijering filtering, anisotropic filtering, etc. (Hayman *et al.*, 2004; Li et al., 2003; Meijering, 2010; Mukherjee and Acton, 2015; Zhou *et al.*, 2015). Nonetheless, the enhancement of neuron images is far from being well established. The neuron morphology contains many subtle features like thin but long neurite fibers and spines. One has to be careful not to destroy these structures through any improper enhancement. Another challenge for image enhancement of 3D neuron images is the computation time, as the procedures applicable for 2D images can easily be too slow for 3D images.

We report in this contribution a data pipeline for the enhancement of 3D dendritic image blocks. The performance of the image enhancement was verified with different figures of merit benchmarking the image quality, the improvement of APP2(all-path-pruning)-based neuron reconstruction, as well as the data volume after a compression.

2 Materials and methods

2.1 Dataset

The study is based on the 3D images of single neurons acquired from 54 mouse brains with the two-photon fluorescence imaging system fMOST (Zheng *et al.*, 2013). The whole-brain images were down-sampled by the scale of two and cropped into blocks of fixed image size ($512 \times 512 \times 256$, *xyz*), each covering the dendritic region of a neuron with the cell body (soma) at the block center. The size of the image blocks was a trade-off between the computation time and the coverage of the entire dendrite. Based on these image blocks, we constructed two datasets for this study. The first was composed of 2500 image blocks randomly selected among the 54 mouse brains, utilized to quantify the performance of the image enhancement. The second dataset contained 605 image blocks as typical examples of image quality ranging from 'good' to 'poor'. The neuron reconstruction was conducted on the second dataset to investigate the improvement via the image enhancement.

2.2 Methods

The workflow of the study is given in Figure 2. Briefly, the image enhancement was conducted to improve the image quality. The performance was qualified via the results of neuron reconstruction, in which the dendritic morphology of the neurons was obtained via APP2 algorithm (Xiao and Peng, 2013). The quantitative assessment was conducted to quantify the performance of the image enhancement. Details of these procedures are given as following.

The image enhancement starts with a sigmoid intensity adjustment according to Equation (1), where I and I^a represent the gray scales of input and adjusted image, respectively (Braun and Fairchild, 1999). The image intensity was normalized to the range 0–1 before the adjustment and rescaled back to 0–255 afterward. The parameter σ was fixed to 3 for all images, while μ was calculated on-the-fly as 25% percentile of the gray scales of the input image (mostly below 10/255). The procedure is followed by subtracting from the image block the minimum of this block along the *z*-axis. A 3D bilateral filtering (Paris and Durand, 2009) was performed afterward, with the window size of $3 \times 3 \times 1$ (*xyz*), the spatial sigma of $1 \times 1 \times 0.33$ (*xyz*) and the range sigma of 35. This helps reduce the noise without significantly harming the neurite structures. Thereafter, we conducted a high-pass filter based on the fast Fourier transform to eliminate the slowly varying background.

$$I^a = \frac{1}{1 + e^{-\sigma(I-\mu)}}. \quad (1)$$

The digital neuron reconstruction was performed with the algorithm APP2. The algorithm was enhanced with the in-house developed procedure of multi-soma correction, for which the publication is under preparation. Details of the APP2 algorithms are referred to Xiao and Peng (2013). The reconstruction was done with the same parameter settings for all image blocks, with or without image enhancement. In particular, the minimal accepted length of the arbor was set as five. The intensity threshold to separate the signal and background was determined automatically as $ave(I) + 0.5 \times st(I)$, where *ave* and *st* denote the average and standard deviation of the image intensity I, respectively.

Besides above-mentioned procedures, we additionally quantified the performance of image enhancement according to different figures of merits that benchmark the image quality. As is well-recognized, to determine the optimal intensity threshold separating the neuron signal form the background (i.e. pre-segmentation) is one

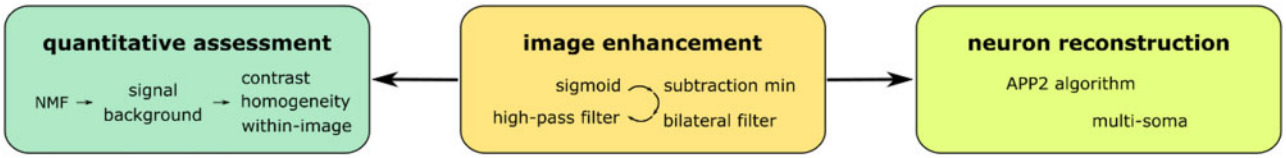

Fig. 2. Workflow of the data pipeline: the improvement of the image quality after image enhancement is evaluated within the step of 'quantitative assessment', where the intensity of both background and foreground is estimated with the NMF (non-negative matrix factorization) method. The improvement of the neuron reconstruction by image enhancement is verified based on the results of the APP2 (all-path-pruning) algorithm

of the key steps in the neuron reconstruction algorithms like APP2. A higher SBC is critical for such pre-segmentation. Nevertheless, it is not uncommon to see the intensities in foreground or background vary largely over a single image, i.e. large dynamic range. This makes it extremely difficult to find the optimal threshold for a good pre-segmentation. Often an adaptive procedure is needed to determine the threshold locally, which increases the computation time significantly. Background that are more homogeneous within an image would be certainly helpful to improve the performance of neuron reconstruction. In a better case, a pre-determined threshold would be sufficient if the background does not vary a lot among different image blocks.

Bearing all the considerations above in mind, we took the SBC, the within-image homogeneity (WIH) and between-image variations (BIV) into consideration as the key aspects of image quality in the scenario of neuron reconstruction. To do so, an image decomposition was conducted to estimate the signal and background for each specific image. This was achieved via the non-negative matrix factorization (NMF) method (Févotte and Idier, 2011) under the independence hypothesis between background and signal of fMOST-based imaging. To be specific, the neurite arbors (signal) are mostly contributed by the fluorescent dyes used in the sparse labeling; while the background mostly comes from the auto-fluorophores or light scattering. It is reasonable to consider the signal and background as physically from different sources and hence independent to each other. The procedure of the NMF decomposition is as following. The average of every 10 image slices along z-axis was calculated and unfolded as 1-dimensioanl vectors. These vectors of each single image block were collected into one matrix. The NMF model was constructed on this matrix with three components, which was used on the entire image block to obtain the decomposed components. The first component was used as the background, while the signal was obtained as the difference between the image block and the background component. We chose to do 3-component NMF as it gives better background-signal separation (i.e. less signal is identified as background) than it does with a 2-component model. The figures of merits for the image quality were calculated from the results of the background-signal estimation. In specific, the SBC was estimated as the difference between the median intensity of the signal and the background. The within-image homogeneity of the background was benchmarked by the entropy $\left(-\sum p(i)\log_2 p(i)\right)$ and uniformity $\left(-\sum p(i)^2\right)$, where $p(i)$ represents the normalized histogram (Van Griethuysen *et al.*, 2017). The within-image homogeneity of the signal was estimated by the relative standard deviation (RSD), i.e. the standard deviation divided by the median value. The standard deviation of each quantity was used to measure the between-image variations. To be clear, only the background under 99% percentile and the signal above 90% percentile were used for the calculation. This helps remove the influence of the residual signal in the estimated background and vice versa, so that the quantification is more reliable.

3 Experiments and results

3.1 Image quality

The example results of the image enhancement are given in Figure 3, wherein the arbor density of the images varies from relatively sparse to relatively dense. Each panel (i.e. a–h) represents one image block, of which the upper left and right subplots give the MIP of the image and the estimated background before enhancement; while the bottom left and right subplots give the MIP of the image and the estimated background after enhancement. The intensity of the estimated background was rescaled for a clear visualization. Apparently, the SBC is largely improved after the enhancement for all images. The tiny features like dendritic spines (see panels a and c) were more visible without the neurite arbors being destroyed. Moreover, the background was well suppressed after the image enhancement and shown to be a lot more heterogeneous both within- and between-image. In addition, the artifacts caused by image-stitching (panels g–h) were well removed after the image enhancement.

The observations above-mentioned were justified by the quantitative comparison based on different quantities benchmarking the image quality. In particular, we re-organized the gray scales of each image as percentiles ranging from 5% to 95%, before and after the image enhancement. The results of the 2500 image blocks are visualized in log-scale as false-color plots in Figure 4a and b. For raw images, the gray scale is seen to change continuously from low to high percentiles and vary significantly among different images. It is hardly possible to find a threshold clearly separating the background and signal for one individual image, not to mention a threshold that suits all images. The situation is changed after the image enhancement, where a sharp change is seen between the low and high gray scale. It thus becomes much easier to find a (global) threshold separating the signal from the background.

More rigorous conclusions can be drawn from the figures of merits shown as violin plots in Figure 4c–h. The quantities were calculated from individual images and collected over all 2500 image blocks for the violin plots. The results from raw and enhanced image blocks were denoted by 'raw' and 'en', with their (global) median marked as blue and red text, respectively. The 'contrast' stands for the SBC; 'med (sg)' and 'med (bg)' for the median intensity of the signal and background; the 'ent (bg)' and 'uni (bg)' for the entropy and uniformity of background; and the 'rsd (sg)' the relative standard deviation of signal. Accordingly, the SBC is significantly improved, with the median five times larger after the enhancement. This is a direct consequence of the enlarged signal and the suppressed background, as is shown by their median intensities in Figure 4d and e. The within-image homogeneity of the background and signal is proven to improve as well. As it is shown in Figure 4e and f, the background features much lower entropy and higher uniformity after the image enhancement; while the signal shows significantly decreased relative standard deviation. In addition, the standard deviation of the background median (med (bg)) over the 2500 image blocks dropped from 3.51 to 0.17, that means a 20-times decrease of the between-image background variation after the image enhancement.

Notably, however, the background for 16 out of the 2500 images did show higher heterogeneous after the image enhancement, featured by a higher entropy or lower uniformity compared to those of raw images. We thoroughly checked these images and collected their results in Supplementary Figure S1. As it will be seen, this happened mostly for images of extremely poor quality, i.e. low contrast or high neuron density. The proposed algorithm may also fail encountering sharp changes in the background like the image blocks containing the edge of the tissue sample (Supplementary Fig. S1e–h). Considering the probability of the occurrence (16 over 2500), however, the performance is by all means acceptable and satisfying.

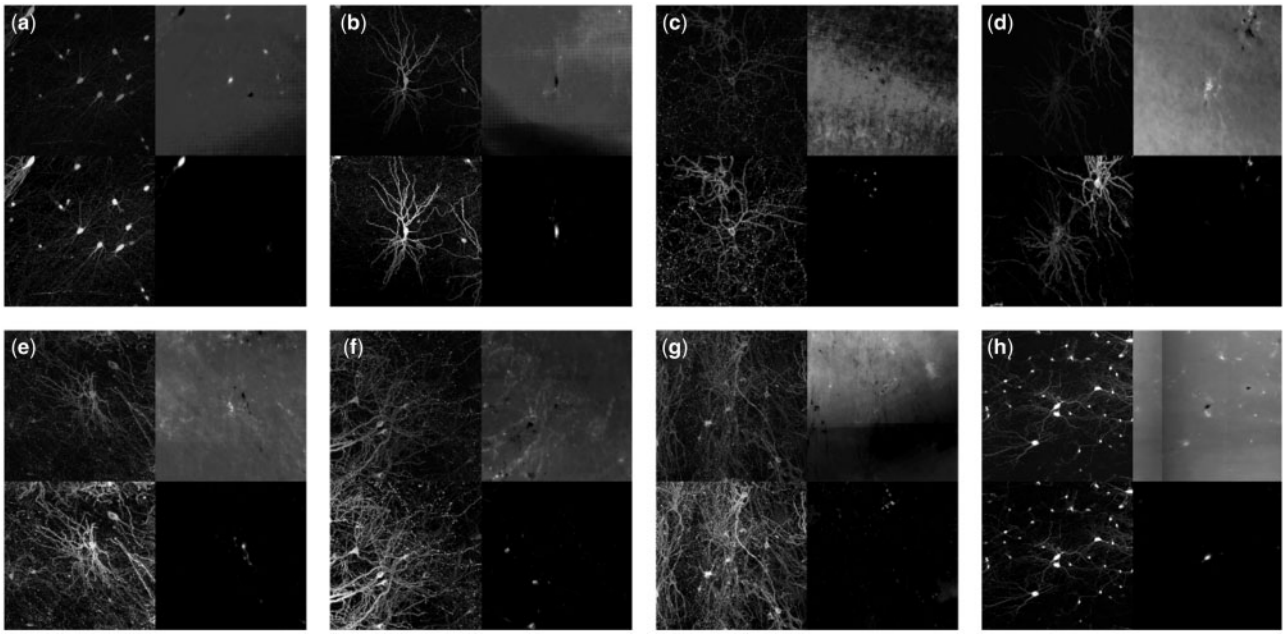

Fig. 3. Example results of image enhancement: each panel (from **a** to **h**) represents the results of one image block. The upper left and right of each panel give the MIP of the image and the estimated background before enhancement; while the bottom left and right of the panel give the MIP of the image and the estimated background after enhancement

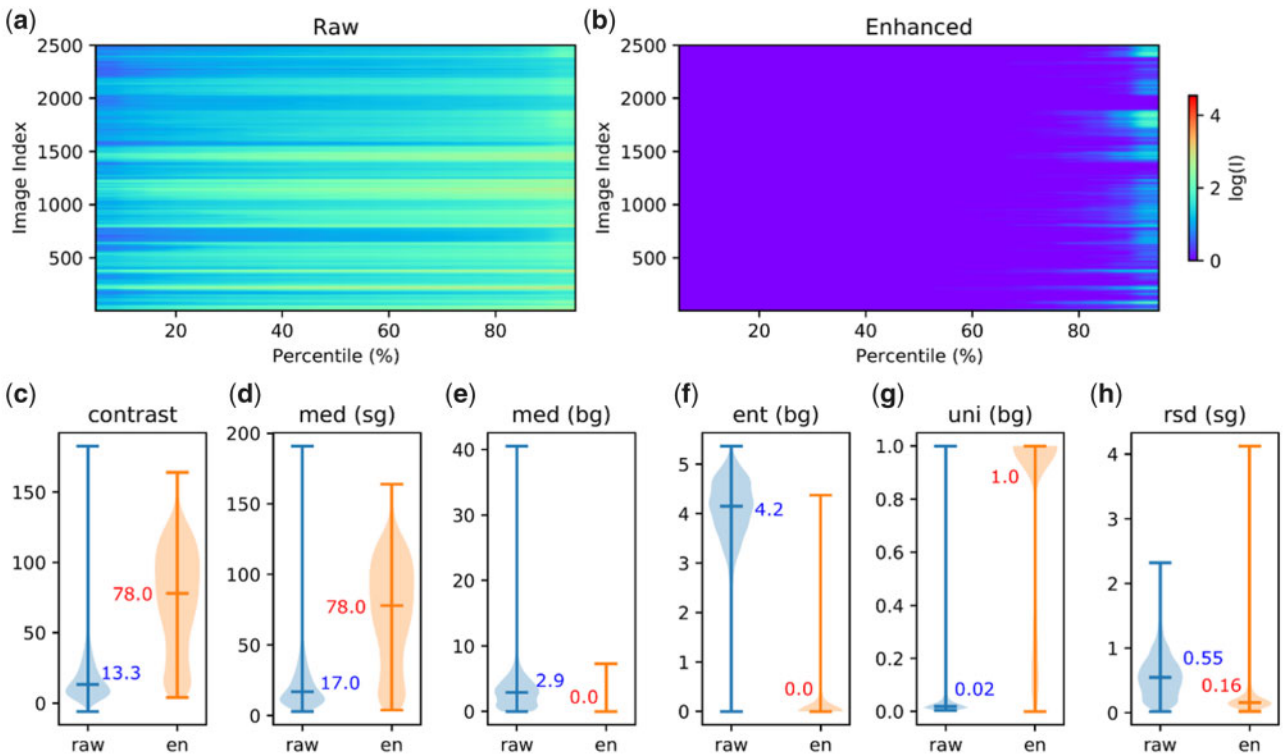

Fig. 4. Results of quantitative assessment. (**a**,**b**) Gray scales at different percentiles for the 2500 images, before and after the image enhancement, respectively. (**c**–**h**) Violin plots of the figures of merit. All values were calculated on individual images and collected from all the 2500 image blocks. The results from raw and enhanced image blocks were denoted by 'raw' and 'en'. Notably, the 'med (sg)' and 'med (bg)' represents the median intensity of the signal and background, respectively. The 'ent(bg)' and 'uni(bg)' means the entropy and uniformity of the background. The 'rsd (sg)' gives the relative standard deviation of signal

3.2 Neuron reconstruction

With higher SBC and improved within- and between-image homogeneity, as were shown above, the image enhancement is expected to improve the neuron reconstruction. To validate, we investigated the APP2-based neuron reconstruction on the 605 image blocks of the second dataset. We particularly checked the results of 27 images where the ground truth from the manual annotation by experienced personnel is available. The reconstructions on raw and enhanced

images are visualized in Supplementary Figure S2 along with the ground truth. No obvious difference was observed if the reconstruction was good enough on raw images like Supplementary Figure S2a–c; and we did remove significant errors like those encircled by boxes in Supplementary Figure S2d–i with marginally smaller chance to introduce errors as marked by arrows in Supplementary Figure S2h–j. Noteworthy, the image quality for these 27 images is generally good and the neuron reconstruction is already close to perfect for raw images. It is thus reasonable not to see much improvement via image enhancement. More significant improvement is observed for images of relatively inadequate quality. This was demonstrated while comparing the reconstruction on raw and enhanced images for all 605 images. The number of reconstructions that are better, comparable or worse reconstructions after the image enhancement are shown in Table 1, in which the 605 images are split into different groups according to their image quality. Typical reconstructions that are denoted as better, worse and comparable are given in Figure 5, Supplementary Figures S3 and S4, respectively. In particular, the neuron reconstruction is considered 'better' if it contains less errors (e.g. distracted by background as Fig. 5a–e, arbors from a neighbor neuron as Fig. 5f–j, missed reconstruction for dim neurite arbors Fig. 5k–u), and 'worse' vice versa. A grade of 'comparable' is given if (i) there is no clear difference (Supplementary Fig. S4a and b), (ii) the reconstruction is inadequate in both cases (Supplementary Fig. S4c) or (iii) a clear judgement is unlikely when too many neurons are present in the neighborhood of the neuron under reconstruction (Supplementary Fig. S4d and e).

Following Table 1, the reconstruction was seen improved for around 1/3 of the image blocks. Typical examples of improvement are shown in Figure 5. The reconstruction was shown to be less disturbed by background (a–e) or the arbors of neighbor neurons (f–j). In addition, features that were too dim to be detected were well reconstructed thanks to the enhanced image contrast (k–q). More

Table 1. The number of image blocks for each group (in total) and how many of them give better/worse/comparable reconstruction after the enhancement than it was without enhancement

	In total	Better	Worse	Comparable
Good	142	47	7	88
Median	336	122	10	204
Poor	127	28	8	91

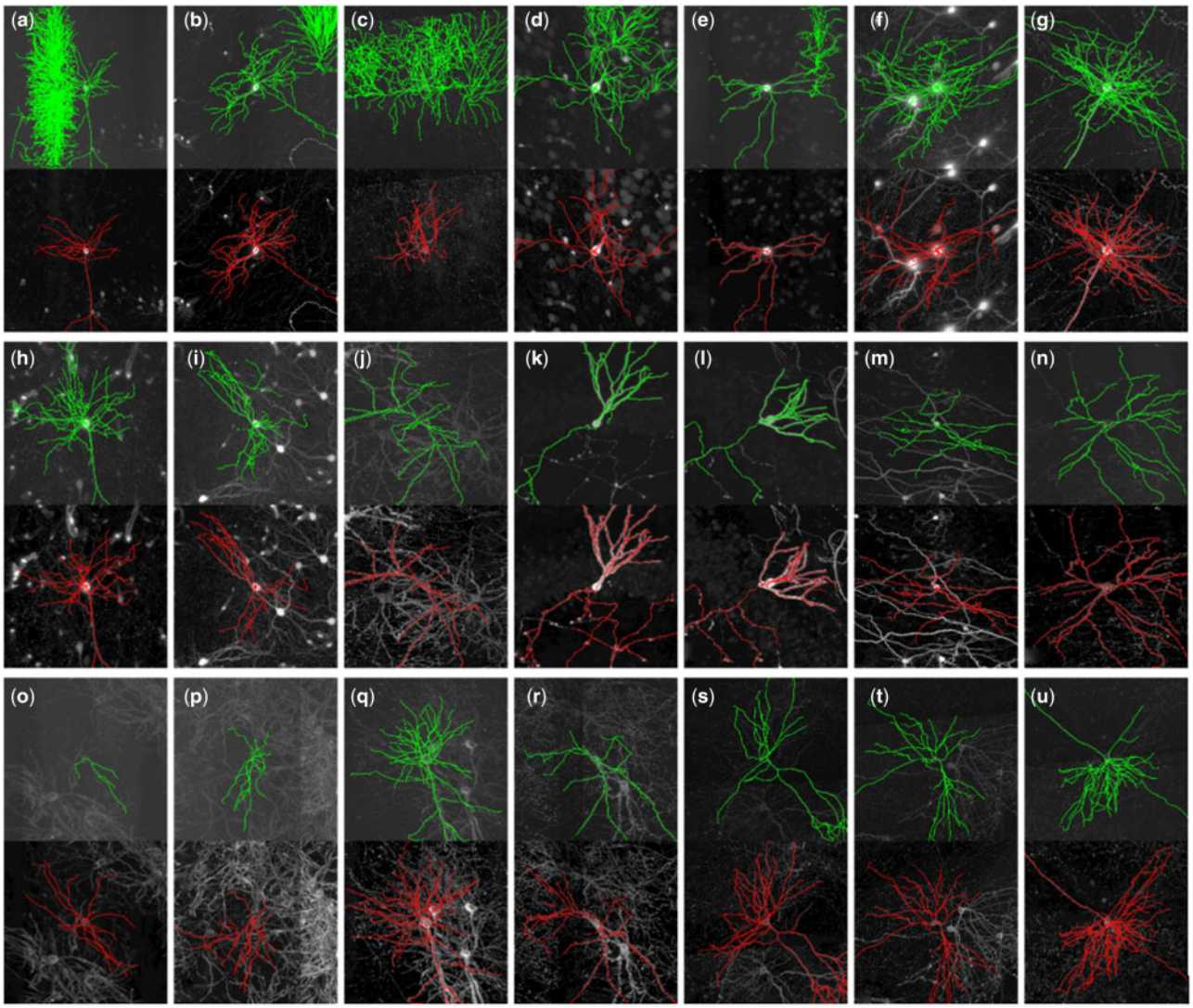

Fig. 5. Typical examples where the neuron reconstruction gets better after the image enhancement (in red) in comparison with that without (in green) the image enhancement. The examples represent different causes of a failed reconstruction on raw images: (**a–e**) disturbance from background or (**f–j**) the arbors of neurons in the neighborhood, (**k–q**) features that were too dim to be detected and (**r–u**) the incomplete reconstruction of neurite arbors due to the sharp change in the background

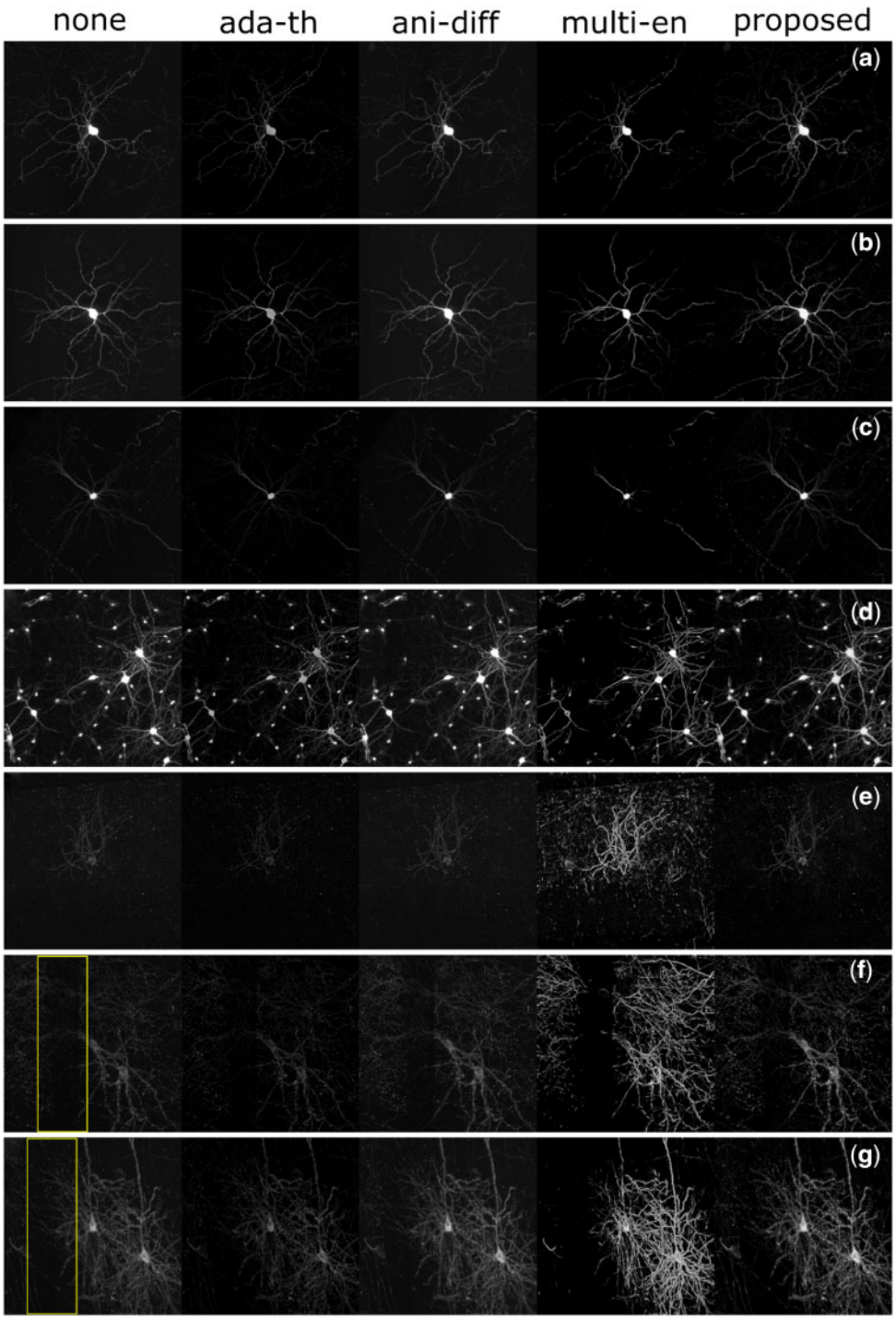

Fig. 6. Example results of image enhancement: the five columns, from left to the right, represent the results with no enhancement, enhanced by adaptive thresholding, anisotropic diffusion, multi-scale enhancement and the proposed method

importantly, the neurite arbor that was not entirely reconstructed due to the sharp change in the background was successfully reconstructed after the image enhancement (r–u). Like it is shown in Supplementary Figure S3, the reconstruction may also become inferior after the image enhancement. The reasons for this include the inadequate removal of the background that contains high-frequency information (Supplementary Fig. S3a–c), as has been discussed previously. In the meantime, the close-by neurite arbors may get connected to each other as the tiny features like spines got enhanced, leading to mistaken reconstruction to other neurons (Supplementary Fig. S3d and e). Nevertheless, the results are well acceptable considering the many cases of improved reconstruction and the small probability of the inadequate background removal (16/2500 according to previous results).

3.3 Performance comparison

As a further verification, we compared our method to three other enhancement approaches based on the 605 images including adaptive thresholding (ada-th), anisotropic diffusion (ani-diff) and multi-scale enhancement (multi-en). All three approaches were implemented via the plugins of the Vaa3D platform. In particular, the

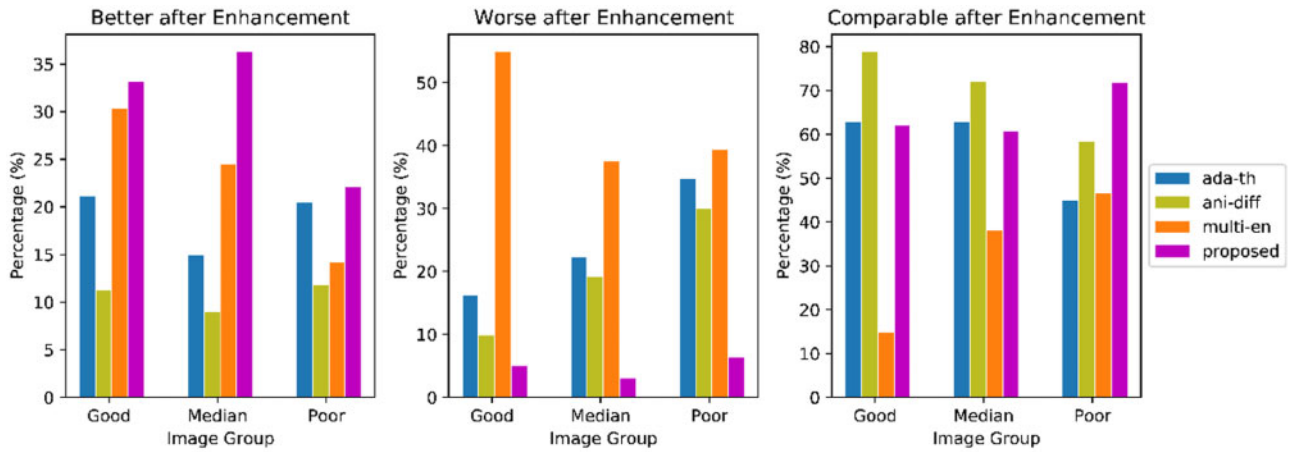

Fig. 7. Percentage of the neuron reconstruction getting better, worse or comparable after being enhanced with different approaches including adaptive threshold, anisotropic diffusion, multi-scale enhancement and the proposed method. The percentage was calculated for three image groups separately as denoted in the *x*-axis (Good, Median, Poor)

multi-scale enhancement was applied with parameters giving generally optimal results on neuron images: the scale of 2, the calibration ratio for GWDT of 0.5, with soma detection and Gaussian blurring. No parameter setting was required for the other two methods. The enhanced images were used for neuron reconstruction with APP2 algorithm, with parameter settings described previously in the section 'Neuron Reconstruction'.

Example results after the image enhancement of different methods are shown in Figure 6. The images are selected to range from 'good' to 'median' quality. As a method to reduce noises, the anisotropic diffusion did little to suppress the background and mostly gives very similar results as for raw images. A significant decrease of background was observed for all other three methods, while the foreground signal was also increased for the multi-scale enhancement and the proposed method. In particular, the neurite arbors are visibly better emphasized by the multi-scale enhancement than they are by the proposed method. This is reasonable as the multi-scale enhancement was designed to selectively enhance tubular structures. However, such selective enhancement may sacrifice the neuron arbors of short lengths as it is shown in Figure 6d. It also risks to introduce artifacts by wrongly enhancing the patterns in the background (Fig. 6e) or to suppress neurite arbors of low intensity (Fig. 6a–c). In particular, a significant information loss is observed for the encircled region in Figure 6e and f, where a stitching effect was caused by the uneven illumination between two subsequent scans of the fMost-based imaging. Without any selective procedure, in contrast, the proposed method is demonstrated to give the best compromise among the signal enhancement, the information loss and the minimal artifact.

Similar to the procedure mentioned beforehand, the neuron reconstruction on the enhanced images was compared to that on raw images for each enhancement approaches. To do so, we calculated the number of image blocks showing better, worse or comparable reconstruction after the enhancement. The results are shown as percentage for the three groups of different image quality (good, median, poor) in each subplot separately in Figure 7. The proposed method is observed to outperform the other three approaches from two aspects. (i) It gives more cases of 'better' reconstructions and less cases of 'worse' reconstruction than all the other three approaches for all three image groups. (ii) It gives significantly more 'better' than 'worse' cases for all three image groups, which occurs for adaptive threshold and anisotropic diffusion only on 'good' images. Despite the many 'better' cases, the multi-scale enhancement 'harms' the reconstruction in more cases. This is mainly because the dim neuron arbors get significantly suppressed and are thus missed for reconstruction (see Fig. 6).

Shown in Figures 8 and 9 are the neuron reconstruction for images of 'good' and 'median' quality, respectively. The results from raw images are given in the first column, followed by those with enhancement by different methods. The images are selected so that the reconstruction looks relatively reasonable in all cases of enhancement. Therefore, we did not present the results from 'poor' quality as the reconstruction was mostly failed even with image enhancement. Generally speaking, the anisotropy diffusion is prone to over-trace and mostly gives similar results as for the raw images. The adaptive thresholding and multi-scale enhancement give an improved reconstruction for images of Figure 8a–c, where the arbors are disturbed by background or surrounded by many disturbing signal. Nonetheless, both approaches show a significant rate of under-tracing in many other cases, as it is observed in the examples of Figure 8d–g. The proposed method is proven to be a good compromise between under- and over-tracing. Despite the remained errors caused by the residual background in Figure 8a–c, the 'redundant' fibers could be well removed without significantly harming the 'true' fibers in many other cases (see Fig. 8d–g). These conclusions are even more clear for images of 'median' quality shown in Figure 9, which again indicates the unique advantage of the proposed method in dealing with images of 'median' quality.

3.4 Compression rate

Besides the performance of neuron reconstruction, another big concern in neuroscience goes to the massive image size considering the exponentially growing data-scale. With this in mind, we randomly picked 100 out of the 2500 image blocks, each with 64 MB volume and compressed into '.zip' files based on the LZMA (Lempel–Ziv–Markov chain) algorithm in the 7z toolkit (Pavlov). The data volumes after compression are summarized in Table 2 for both individual image blocks and the total amount. In total, the data volume was decreased from 6400 to 960 MB and 241 MB for raw and enhanced images, respectively. This means an average compression rate of 15.0% and 3.8%, almost 4 times decrease via the image enhancement. In the best case, the compression rate of a single image block was decreased almost 20 times from 6.9% for raw to 0.35% after being enhanced. The proposed image enhancement is hence potential to reduce the cost of data storage and transfer.

4 Conclusions and discussion

In this contribution, we proposed a pipeline of image enhancement to improve the quality of 3D neurite images. The method is designed to simultaneously suppress the background and enhance the foreground. This improves the SBC as well as the within- and between-image homogeneity, as was demonstrated quantitatively by the different figures of merits benchmarking the image quality. The method is shown to largely narrow down the dynamic range of the foreground signal, which helps to separate the foreground from the background during the subsequent reconstruction. Therefore, it has

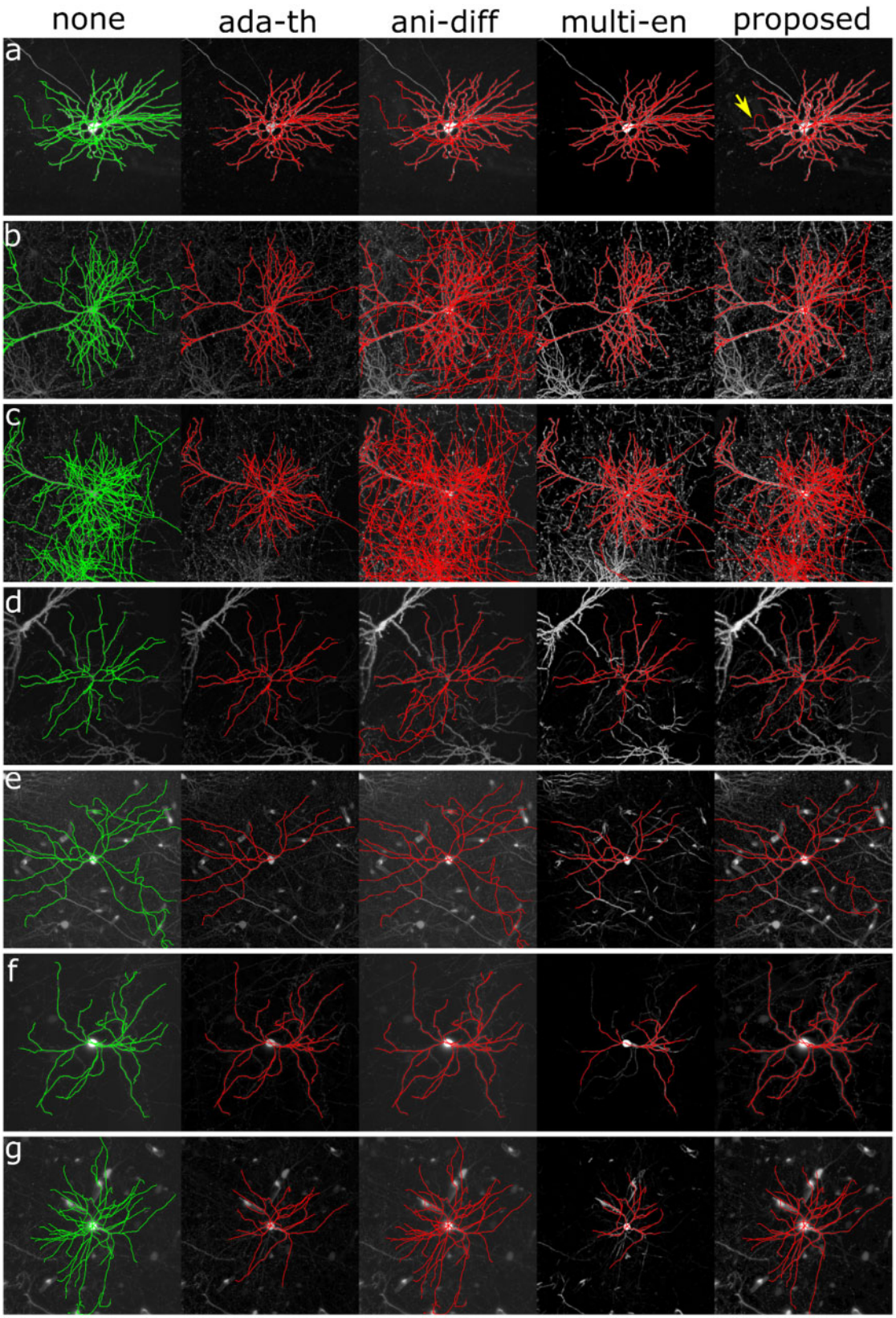

Fig. 8. Results of the neuron reconstruction on images of 'good' quality, i.e. relatively sparse neuron arbors and flat background. The five columns, from left to right, represent the cases without image enhancement ('none'), and with enhancement by the four different approaches

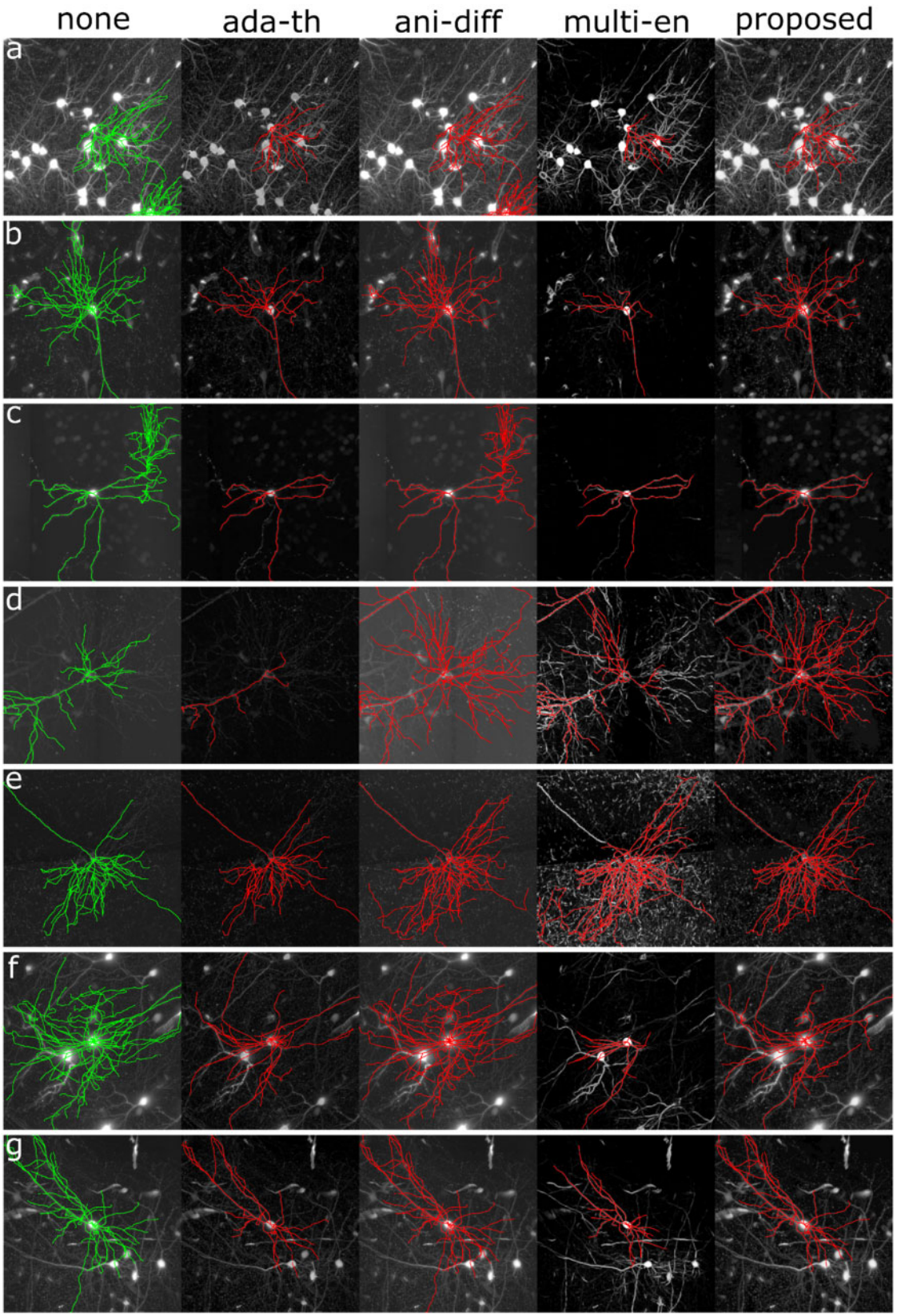

Fig. 9. Results of the neuron reconstruction on images of 'median' quality, i.e. relatively dense neuron arbors or disturbing background. The five columns, from left to right, represent the cases without image enhancement ('none'), and with enhancement by the four different approaches

Table 2. Image size and compression rate via LZMA compression

	Total	Average rate	Single image	Single rate
Raw	960 MB	15.0%	[4.5 MB, 30.8 MB]	[6.9%, 43.7%]
Enhanced	241 MB	3.8%	[231 KB, 13.6 MB]	[0.35%, 19.2%]

shown significant advantages to improve the neuron reconstruction, particularly for images of 'median' quality. In addition, we could see 5 times of increase in the compression rate for 7z compression comparing the enhanced to raw images, making the method potentially advantageous to reduce the cost in data storage and transfer. Unlike the methods that selectively enhance the tubular structures to be used for neuron images (e.g. multi-scale enhancement), the proposed method is not limited to enhancing any specific structures. In fact, it shows also great performance in enhancing tiny features like dendrite spines (see Figs 3 and 6). Hence it is very likely helpful in the scenarios of bouton or spine detection as well. However, by narrowing down the dynamic range of the foreground signal, the method may fall short for quantitative analysis where the intensity of the neurite arbors is important. Further improvement of the method also goes to its capability to deal with sharp changes in the background, where it introduces artifacts at current stage. This could be done by additionally taking the local information of the background, instead of only global information as it is right now.

Our method was implemented in C++ as a plugin program on the Vaa3D platform (Peng *et al.*, 2010). The computation, involving image import and results saving, takes by average 15 s per image with the size of $512 \times 512 \times 256$, *xyz*, on a Windows machine with Intel (R) i9-10900K 3.7 GHZ CPU, largely faster than the approximately 150 s for the multi-scale enhancement. Embedding the method on the fly and hence leverage the procedure of manual/automatic reconstruction and even image acquisition can be valuable work to do in the future.

Funding

The study was funded by Southeast University Research Startup Fund [4350272071] for L.D. and the Fundamental Research Funds for the Central Universities [2242021k30046].

Conflict of Interest: none declared.

References

Batson,J. and Royer,L. (2019) Noise2self: blind denoising by self-supervision. In: *International Conference on Machine Learning*. PMLR, Long Beach, California, USA.

Braun,G.J. and Fairchild,M.D. (1999) Image lightness rescaling using sigmoidal contrast enhancement functions. *J. Electronic Imaging*, **8**, 380–393.

Buchholz,T.-O. *et al.* (2019) Cryo-care: content-aware image restoration for cryo-transmission electron microscopy data. In: *2019 IEEE 16th International Symposium on Biomedical Imaging (ISBI 2019)*. IEEE, Venice, Italy.

Chernavskaia,O. *et al.* (2017) Correction of mosaicking artifacts in multimodal images caused by uneven illumination. *J. Chemometrics*, **31**, e2901.

Dabov,K. *et al.* (2006) Image denoising with block-matching and 3D filtering. In: *Proceedings Volume 6064, Image Processing: Algorithms and Systems, Neural Networks, and Machine Learning, Electronic Imaging 2006*, San Jose, California, USA.

Févotte,C. and Idier,J. (2011) Algorithms for nonnegative matrix factorization with the β-divergence. *Neural Comput.*, **23**, 2421–2456.

Hayman,M. *et al.* (2004) Enhanced neurite outgrowth by human neurons grown on solid three-dimensional scaffolds. *Biochem. Biophys. Res. Commun.*, **314**, 483–488.

Krull,A. *et al.* (2020) Probabilistic noise2void: unsupervised content-aware denoising. *Front. Comput. Sci.*, **2**, 5.

Laine,S. *et al.* (2019) High-Quality Self-Supervised Deep Image Denoising, In: *33rd Conference on Neural Information Processing Systems (NeurIPS 2019)*, Vancouver, Canada.

Lehtinen,J. *et al.* (2018) Noise2noise: learning image restoration without clean data. *arXiv*. preprint arXiv:1803.04189.

Li,Q. *et al.* (2003) Selective enhancement filters for nodules, vessels, and airway walls in two-and three-dimensional CT scans. *Med. Phys.*, **30**, 2040–2051.

Liang,H. *et al.* (2017) Content-aware neuron image enhancement. In: *2017 IEEE International Conference on Image Processing (ICIP)*. IEEE, Beijing, China.

Meijering,E. (2010) Neuron tracing in perspective. *Cytometry A*, **77**, 693–704.

Mukherjee,S. and Acton,S.T. (2015) Oriented filters for vessel contrast enhancement with local directional evidence. In: *2015 IEEE 12th International Symposium on Biomedical Imaging (ISBI)*. IEEE, Brooklyn, New York, USA.

Paris,S. and Durand,F. (2009) A fast approximation of the bilateral filter using a signal processing approach. *Int. J. Comput. Vis.*, **81**, 24–52.

Pavlov,I. 7z format. https://www.7-zip.org/7z.html(March, 2021, date last accessed).

Peng,H. *et al.* (2010) V3D enables real-time 3D visualization and quantitative analysis of large-scale biological image data sets. *Nat. Biotechnol.*, **28**, 348–353.

Peng,T. *et al.* (2017) A BaSiC tool for background and shading correction of optical microscopy images. *Nat. Commun.*, **8**, 14836–14837.

Smith,K. *et al.* (2015) CIDRE: an illumination-correction method for optical microscopy. *Nat. Methods*, **12**, 404–406.

Svoboda,K. (2011) The past, present, and future of single neuron reconstruction. *Neuroinformatics*, **9**, 97–98.

Van Griethuysen,J.J. *et al.* (2017) Computational radiomics system to decode the radiographic phenotype. *Cancer Res.*, **77**, e104–e107.

Xiao,H. and Peng,H. (2013) APP2: automatic tracing of 3D neuron morphology based on hierarchical pruning of a gray-weighted image distance-tree. *Bioinformatics*, **29**, 1448–1454.

Xu,J. *et al.* (2018) A trilateral weighted sparse coding scheme for real-world image denoising. In: *Proceedings of the European Conference on Computer Vision (ECCV)*, Munich, Germany.

Zheng,T. *et al.* (2013) Visualization of brain circuits using two-photon fluorescence micro-optical sectioning tomography. *Opt. Express*, **21**, 9839–9850.

Zhou,Z. *et al.* (2015) Adaptive image enhancement for tracing 3D morphologies of neurons and brain vasculatures. *Neuroinformatics*, **13**, 153–166.

Zhu,J.-Y. *et al.* (2017) Unpaired image-to-image translation using cycle-consistent adversarial networks. In: *Proceedings of the IEEE International Conference on Computer Vision*, Venice, Italy.